Crystal symmetry of $La_3Cu_2VO_9$ and $La_4Cu_3MoO_{12}$ derived from the $YAlO_3$ hexagonal structure by transmission electron microscopy

Sylvie Malo [a], Douglas A. Vander Griend [a], Kenneth R. Poeppelmeier [a,*],
Yanguo Wang [b], Vinayak P. Dravid [c]

[a] *Department of Chemistry, Northwestern University, 2145 Sheridan Road, Evanston, Illinois 60208-3113, USA*
[b] *Beijing Laboratory of Electron Microscopy, Institute of Physics and Center for Condensed Matter Physics, Chinese Academy of Sciences,
P.O. Box 2724, Beijing 100080, PR China*
[c] *Department of Materials Science and Engineering, Northwestern University, 2137 Sheridan Road, Evanston, Illinois 60208-3108, USA*

Dedicated to Professor Michel Tournoux on the occasion of his retirement

Abstract

$La_4Cu_3MoO_{12}$ and $La_3Cu_2VO_9$, homeotypes of $YAlO_3$, an ABO_3 hexagonal phase, have been investigated using a variety of transmission electron microscopy techniques. Both compounds possess the same hexagonal subcell but exhibit different supercells. The unit cell parameters and symmetry have been determined using selected area and convergent beam electron diffraction techniques. For $La_3Cu_2VO_9$, electron energy loss spectroscopy and energy dispersive X-ray spectroscopy were used to determine the oxidation-state of vanadium and the cation stoichiometry, respectively, which conforms to $La_3Cu_2VO_9$. This paper highlights the need for multitechnique approaches to complex oxide structures. © 2001 Éditions scientifiques et médicales Elsevier SAS. All rights reserved.

Keywords: $La_3Cu_2VO_9$; $La_4Cu_3MoO_{12}$; Transmission electron microscopy; Electron diffraction; EELS

1. Introduction

The development of useful oxides requires an understanding of the complex relationships between stoichiometry, structure and properties. Structural determination remains a major step in the study of materials chemistry. ABO_3 compounds have attracted considerable attention owing to interesting physical properties such as high temperature superconductivity and colossal magneto-resistance [1]. The

ABO_3 structural phase diagram constructed by Giaquinta et al. maps stoichiometry to structure based on ionic radii and bond ionicities [2]. X-ray and neutron powder diffraction techniques have been indispensable in determining average structures but the scattering efficiencies are often insufficient to determine the crystal symmetry unambiguously. For these reasons, transmission electron microscopy (TEM), and in particular electron diffraction, has become a useful tool in the study of the solid state of materials.

We report here a study by electron diffraction and spectroscopies [electron energy loss spectroscopy

(EELS) and energy dispersive X-ray spectroscopy (EDS)] performed on two samples, $La_4Cu_3MoO_{12}$ and $La_3Cu_2VO_9$.

2. Experimental

The molybdenum and vanadium cuprates, $La_4Cu_3MoO_{12}$ and $La_3Cu_2VO_9$, were prepared as previously reported, starting from the stoichiometric ratio of La_2O_3, CuO, MoO_3 and VO_2, fired at high temperature and slowly cooled to room temperature [3,4].

For the TEM study, the samples were crushed in alcohol and the small flakes deposited on holey carbon grids. The electron diffraction was performed on a Hitachi-8100 operated at 200 kV. The spectroscopy studies were carried out on a Hitachi HF2000 equipped with a cold-field emission gun. The cationic composition was verified by EDS performed with Oxford's Pentafet Link detector with QX2000 processor/system. The EELS spectra were acquired at 200 kV with a Gatan 666 parallel spectrometer in diffraction mode. The energy resolution of the spectrometer is around 0.5 eV (full width at half maximum).

3. Results and discussion

The powder X-ray diffraction (XRD) data did not show any impurity phases either for the molybdate or the vanadate sample. Their XRD patterns resemble that of $YAlO_3$ with additional reflections (Fig. 1) [5]. Therefore, in order to determine the supercell with the cell parameters and symmetry, we have performed a complete structural characterization by electron diffraction.

The TEM study is performed on very small crystallites from powder samples and does not require large single crystals. TEM can be used in two major modes: diffraction and image. Using the TEM in diffraction mode allows 2D diffraction patterns to be recorded. The beam size, the beam convergence and the camera length, are three different parameters that can be adjusted to obtain different electron diffraction patterns, which provide different information concerning the crystal symmetry. The selected area electron diffraction (SAED) is characterized by a large parallel incident beam.

Based on specific SAED patterns, the reciprocal space is reconstructed which gives the extinction conditions and the lattice parameters. Convergent beam electron diffraction (CBED) is characterized by a relatively small-converged beam. Three different types of CBED patterns can be obtained depending on the camera length and the beam focus: the zero order Laüe zone (ZOLZ), the high order Laüe zone (HOLZ) and the whole pattern. The ZOLZ patterns, recorded using a medium camera length, exhibit for some zone axes the Gjønnes-Moodie (G-M) lines from which additional translation symmetry elements such as screw axes and glide planes can be deduced [6]. With a small camera length, CBED patterns exhibit the HOLZ rings, from which the unit cell can be determined. Whole patterns (WP), recorded using a small camera length and a small convergence of beam, evidence mirror planes. Together these diffraction techniques can be used to determine the symmetry and space group of new compounds.

The SAED patterns for both $La_4Cu_3MoO_{12}$ and $La_3Cu_2VO_9$ show a set of intense diffraction spots characteristic of the hexagonal subcell (see Fig. 7,

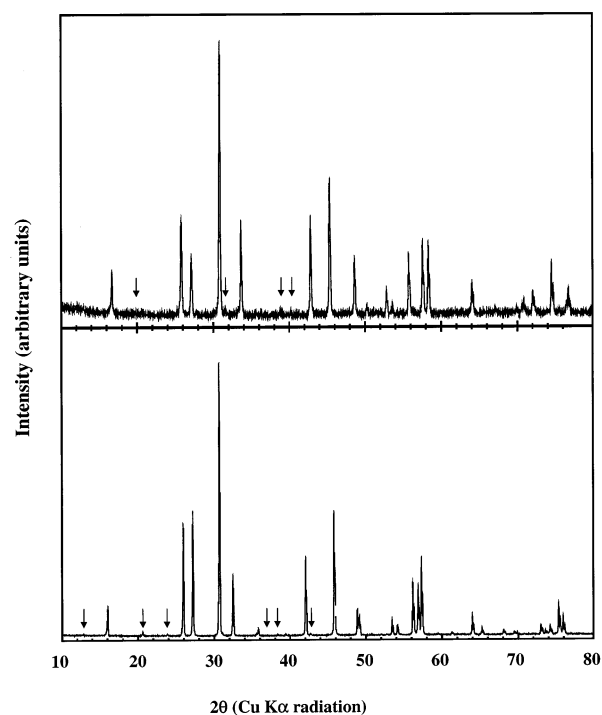Fig. 1. Powder X-ray pattern for (a) $La_4Cu_3MoO_{12}$, and (b) $La_3Cu_2VO_9$. Arrows mark superstructural peaks.

(a)

(b)

(c)
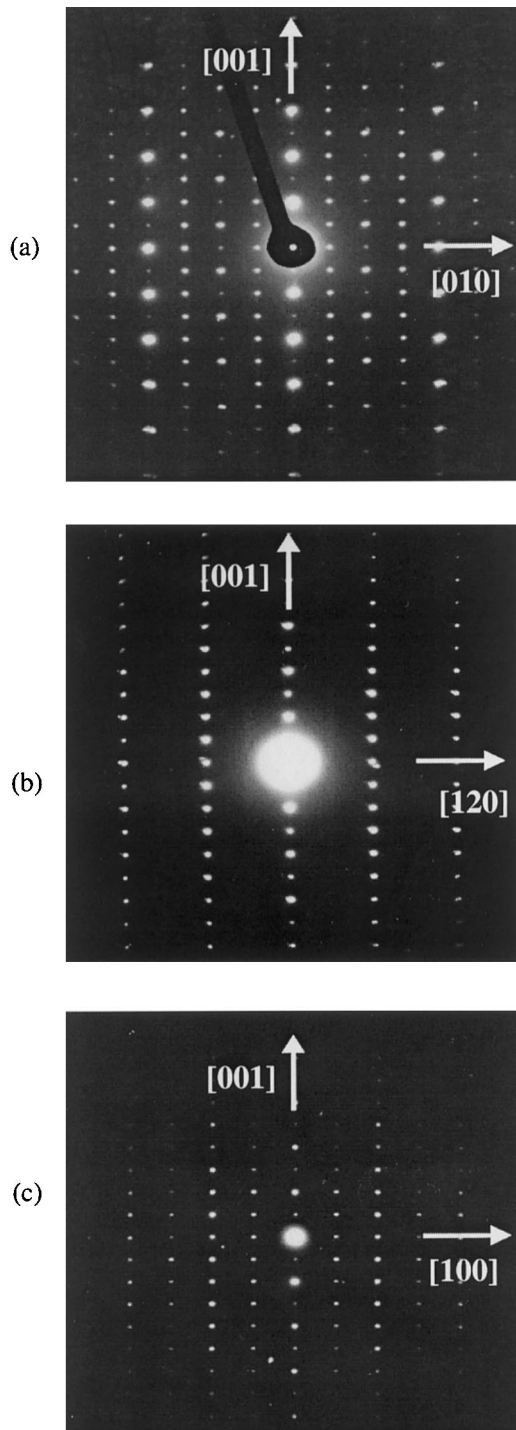
Fig. 2. SAED patterns of $La_4Cu_3MoO_{12}$ oriented (a) [100], (b) [$2\bar{1}0$], and (c) [010].

representing $La_3Cu_2VO_9$ pattern) ($a \approx 4$ Å and $c \approx 11$ Å) classically observed for the rare earth hexagonal $YAlO_3$ structure type. However, extra, weaker reflections for both samples are also systematically observed.

3.1. $La_4Cu_3MoO_{12}$

For the molybdate sample, the additional reflections, which are not compatible with hexagonal symmetry, define a monoclinic or orthorhombic cell with $a \approx 8$ Å, $b \approx 7$ Å $\approx 4.0\sqrt{3}$, $c \approx 11$ Å and $\gamma \approx 90°$. The reconstruction of reciprocal space based on collecting specific SAED patterns indicated only one condition for forbidden reflection: $00l$: $l \neq 2n$. This extinction condition for a monoclinic or orthorhombic symmetry implies a 2_1-screw axis along the c-axis. Therefore, according to the international tables for crystallography [7], the possible space groups are $P112_1$, $P112_1/m$ and $P222_1$. Fig. 2 shows [100], [$2\bar{1}0$] and [010] SAED patterns.

Additional symmetry elements such as screw axes and mirror planes were deduced from a CBED study by observing the G-M lines and by determining WP symmetries, respectively [8,9]. The G-M lines refer to the dynamical absences in the kinetically forbidden reflections and appear as dark bands or crosses in some kinematically forbidden reflections, shown schematically in Fig. 3. Dark bands indicate that the electron beam is either parallel to a glide plane or
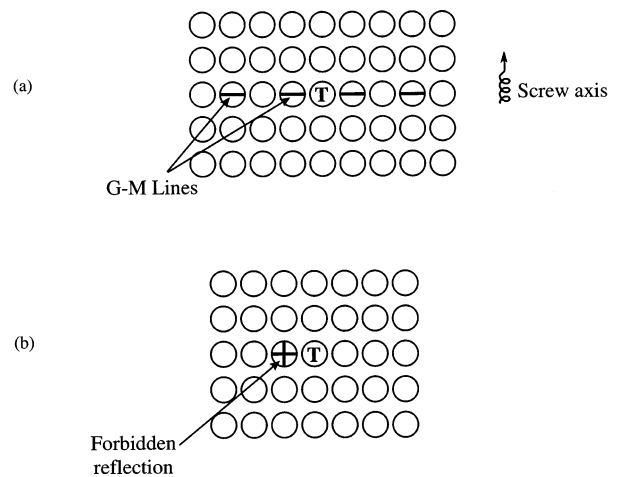

Fig. 3. Schematic representation of G-M lines (a) indicating a screw axis perpendicular to the beam (b) black crosses indicating forbidden reflections.
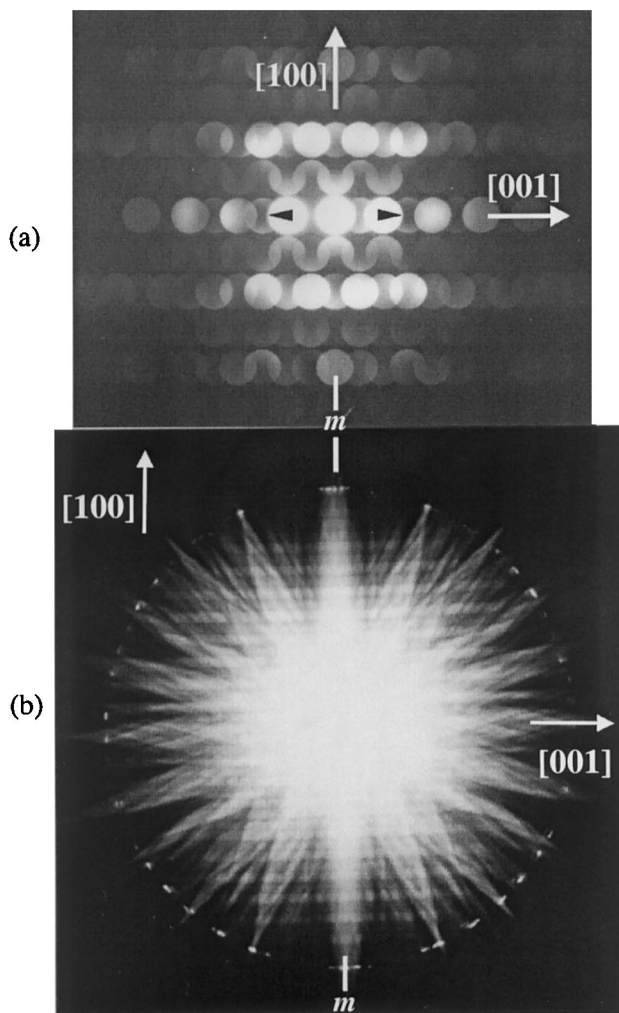
Fig. 4. [010] CBED pattern of $La_4Cu_3MoO_{12}$. (a) ZOLZ pattern. The black arrows indicate the G-M lines visible in the 00*l* discs for *l* odd. (b) Whole pattern exhibiting a mirror plane perpendicular to the *c*-axis.

perpendicular to a screw axis in the crystal, and the black crosses refer to forbidden reflections.

The ZOLZ-CBED pattern taken along the [010] zone axis shows G-M lines in the 00*l* discs for *l* odd, indicated by black arrows on Fig. 4(a). According to the tables established by Steeds et al. [10], the G-M lines confirm the presence of a 2_1 screw axis parallel to the *c*-axis and the forbidden reflections (00*l*: $l \neq 2n$). Again, the three possible space groups are $P112_1$, $P112_1/m$ and $P222_1$, the [010] WP exhibits a mirror plane (Fig. 4(b)) perpendicular to the *c*-axis, which indicates that $P112_1/m$ (no. 11) is the correct space group.

3.2. $La_3Cu_2VO_9$

Unlike the molybdate compound, thermogravimetric analysis (TGA) could not be used to successfully determine the stoichiometry of the vanadate sample owing to the ambivalence of the oxidation state of vanadium. EDS was used to ascertain the cationic ratio and EELS to determine the vanadium oxidation state after synthesis (vanadium(IV) oxide was used as starting material).

EDS analyses established the cationic ratios La:V of 2.9(2) and Cu:V of 1.99(9) in agreement with the synthetic composition.

The EELS spectra were recorded at the L_3/L_2 edge of vanadium. For this study, we focused on the high-loss regions, which contain the vanadium $L_{2,3}$ peaks and oxygen K peak (Fig. 5). The vanadium L_2 and L_3 peaks represent electronic transitions from vanadium $2p_{1/2}$ and $2p_{3/2}$ states to molecular orbitals with 3d character [11]. The oxygen *k*-edge, which spreads between 525 and 550 eV, represents transition from the oxygen 1s state to molecular orbitals with oxygen 2p character. At higher energy, we observe the lanthanum $M_{4,5}$ peaks (Fig. 6). Previous studies reported that the L_3/L_2 ratio increases as the
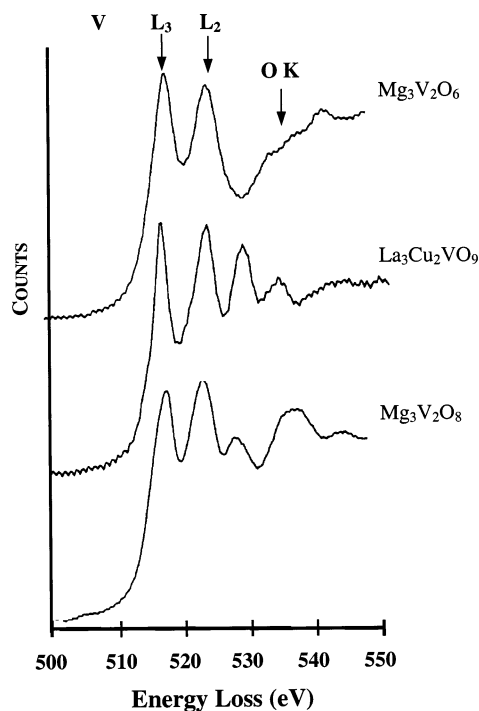

Fig. 5. The region from 500 to 550 eV in energy loss spectra of (a) $Mg_3V_2O_6$, (b) $La_3Cu_2VO_9$ and (c) $Mg_3V_2O_8$.
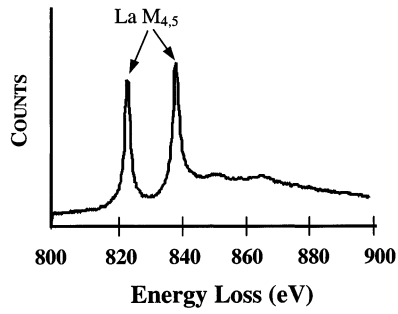
Fig. 6. The region from 800 to 900 eV in energy loss spectra of $La_3Cu_2VO_9$.

Table 1
Experimental values for the ratios between background-subtracted, integrated intensities of V L_3 and V L_2 peaks

Phase	V L_3/L_2
$Mg_3V_2O_6$	0.90(8)
$Mg_3V_2O_8$	0.72(4)
$La_3Cu_2VO_9$	0.69(6)

oxidation states of transition metals such as vanadium and manganese decreases and therefore can be used to determine the oxidation state of cations in 3d transition metal-oxides [12,13]. In order to determine the oxidation state of vanadium in our sample, the spectra at the L_3/L_2 edge were recorded for $Mg_3V_2O_6$ and $Mg_3V_2O_8$ where vanadium exhibits the +3 and +5 oxidation states, respectively [14]. In both magnesium vanadium oxides, the vanadium oxidation state was also evidenced by XRD and IR studies. All spectra were obtained from 500 to 550 eV integrated using Peakfit4® program. The L_3/L_2 ratio obtained for $La_3Cu_2VO_9$, $Mg_3V_2O_6$ and $Mg_3V_2O_8$ are listed in Table 1. The values obtained for $La_3Cu_2VO_9$ are equal within the experimental error to the ones obtained for $Mg_3V_2O_8$ and indicate that vanadium is in the +5 oxidation-state. The EELS study, com-

bined with the EDS results, confirms the stoichiometry $La_3Cu_2VO_9$ for the hexagonal phase.

With the confirmation of the stoichiometry, we now deal with the structural study. For the vanadate sample, the system of additional spots implies a new hexagonal cell with $a \approx 14.4$ Å and $c \approx 10.7$ Å, which was previously reported by Jansson et al. [15].

The HOLZ rings, observed on CBED patterns, were used to verify the supercell. The real lattice spacing (H_m^{-1}) parallel to the beam direction can be expressed by the measured radius of the HOLZ ring r (mm) and the camera constant λL (nm mm):

$$H_m^{-1} = \left(\frac{2}{\lambda}\right)\left(\frac{\lambda L}{r}\right)^2 \tag{1}$$

This value can be compared to the theoretical one (H_c^{-1}) calculated from equations developed from reciprocal lattice theory [16,17]. For hexagonal systems:

$$H_c^{-1} = (a^2(U^2 + V^2 - UV) + c^2 W^2)^{1/2} \tag{2}$$

The calculated value H_c^{-1} must be an integer multiple (n) of the measured spacing H_m^{-1}, where n represents the order of the Laüe zone:

$$H_c^{-1} = n \times H_m^{-1} \tag{3}$$

Table 2 lists the measured and calculated H^{-1} based on the hexagonal supercell. The agreement between the values confirms the validity of our hexagonal cell and indicates that a larger supercell is not merited.

The reconstruction of the reciprocal space deduced from many SAED patterns obtained by tilting along the $a*$ and $c*$ axes indicated only one condition for forbidden reflections, $000l$: $l \neq 2n$. In hexagonal systems, this extinction condition represents a 6_3-screw axis along the c direction and therefore three space groups are possible: $P6_3$, $P6_3/m$ and $P6_322$. Fig. 7 exhibits the [0001], [11$\bar{2}$0] and [1$\bar{1}$00] SAED patterns.

Table 2
Calculated and measured layer spacings (H^{-1}) from CBED patterns

Crystal orientation	Laüe zone order (n)	Calculated H_c^{-1} (nm)	Measured H_m^{-1} (nm)
$2\bar{1}0$	1	3.81	3.80(6)
112	1	2.58	2.58(5)
114	1	4.5	4.6(2)
$3\bar{1}0$	1	5.2	5.1(2)
$1\bar{1}0$	1	2.49	2.49(3)

(a)

(b)

(c)
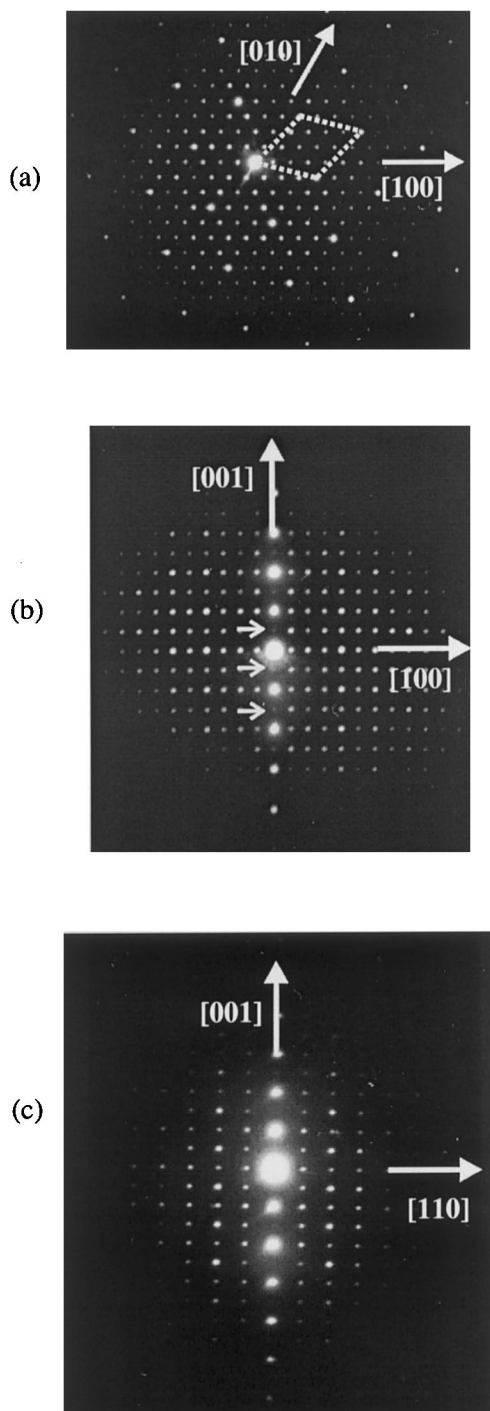
Fig. 7. (a) [0001], (b) [11$\bar{2}$0] and (c) [1$\bar{1}$00] SAED patterns of La$_3$Cu$_2$VO$_9$. The small arrows on Fig. 2(b) indicate forbidden spots visible owing to double diffraction.
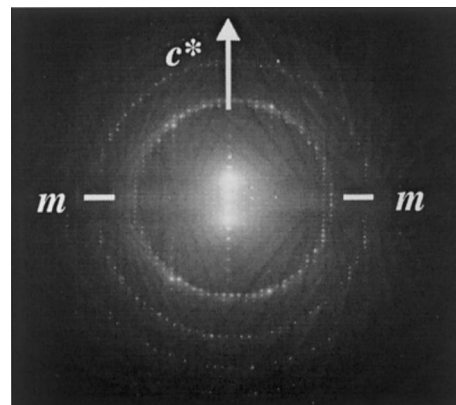

Fig. 8. [1$\bar{1}$00] zone-axis whole pattern from La$_3$Cu$_2$VO$_9$ showing the mirror plane perpendicular to the c-axis.

The 000l spots with l odd are weakly visible in some SAED patterns (indicated by small arrows on Fig. 7(b)) owing to dynamical scattering events, commonly called double diffraction.

The three possible space groups correspond to the point groups 6, 6/m and 622, respectively, which are characterized by three distinct WP symmetries [18]. The WP taken along [1$\bar{1}$00] shows a mirror plane perpendicular to the c-axis (Fig. 8), so the correct space group is $P6_3/m$.

4. Conclusion

The symmetry and the lattice parameters of La$_4$Cu$_3$MoO$_{12}$ and La$_3$Cu$_2$VO$_9$ have been determined unambiguously from electron diffraction microscopy. Thus, La$_4$Cu$_3$MoO$_{12}$ crystallizes in a monoclinic cell with $a \approx 8$ Å, $b \approx 7$ Å $\approx 4.0\sqrt{3}$, $c \approx 11$ Å, $\gamma \approx 90°$ and P112$_1$/m symmetry, and La$_3$Cu$_2$VO$_9$ in a hexagonal cell with $a \approx 14.4$ Å, $c \approx 10.7$ Å and $P6_3/m$ symmetry. For the latter compound, related spectroscopy studies (EDS and EELS) confirm the composition of the hexagonal phase and evidenced the +5 oxidation-state of vanadium. Knowing the unit cell parameters, symmetry and composition has led to the successful determination of the atomic positions by Rietveld method from X-ray or neutron powder diffraction data [3,4]. This study underscores the need for diverse transmission electron microscopy techniques in unraveling complex oxide structure.

Acknowledgements

References

[1] C.N.R. Rao, J. Mater. Chem. 9 (1999) 1.
[2] D.M. Giaquinta, H.-C. zur Loye, Chem. Mater. 6 (1994) 365.
[3] D.A. Vander Griend, S. Boudin, V. Caignaert, K.R. Poeppelmeier, Y. Wang, V.P. Dravid, M. Azuma, M. Takano, Z. Hu, J.D. Jorgensen, J. Am. Chem. Soc. 121 (1999) 4787.
[4] D.A. Vander Griend, S. Malo, S. Barry, N. Dabousseh, K.R. Poeppelmeier, V.P. Dravid, Solid State Sciences, submitted.
[5] F. Bertaut, J. Mareschal, Compte Rendu des Sciences 257 (1963) 867.
[6] J. Gjønne, A.F. Moodie, Acta Cryst. 19 (1965) 65.
[7] T. Hahn, International Tables for Crystallography. D. Reidel Publishing Company: Dordrecht, (1983)
[8] J. Gjønne, A.F. Moodie, Acta Cryst. 19 (1965) 65.
[9] D.B. Williams, C. Barry Carter, Transmission Electron Microscopy, Plenum Press, Chapter 21 (1996) 319.
[10] J.W. Steeds, R. Vincent, J. Appl. Cryst. 16 (1983) 317.
[11] C.C. Ahn, O.L. Krivanek, EELS Atlas (Center for Solid State Science, Arizona State university, Tempe, AZ) (1983).
[12] X.W. Lin, Y.Y. Wang, V.P. Dravid, P.M. Michakalos, M.C. Kung, Phys. Rev. B 47 (1993) 3477.
[13] J.H. Rask, B.A. Miner, P.R. Buseck, Ultramicroscopy 21 (1987) 321.
[14] X. Wang, H. Zhang, W. Sinkler, K.R. Poeppelmeier, L.D. Marks, J. Alloys Comp. 270 (1998) 88.
[15] K. Jansson, I. Bryntse, Y. Teraoka, Mater. Res. Bull. 31 (1996) 827.
[16] M. Raghavan, J.C. Scanlon, J.W. Steeds, Met. Trans. 15A (1984) 1299.
[17] R. Ayer, J. Electron Microsc. Tech. 13 (1989) 16.
[18] B.F. Buxton, J.A. Eades, J.W. Steeds, G.M. Rackham, Phil. Trans. Roy. Soc. 281 (1976) 181.